JOURNAL OF SOLID STATE CHEMISTRY 113, 327–344 (1994)

Structural Aspects of $Bi_{2-x}Pb_xSr_{3.5}Cu_2(CO_3)O_{8-\delta}$ for $0 \leq x \leq 0.75$: An Electron Microscopy Study

X. F. Zhang,*[,1] G. Van Tendeloo,* S. Amelinckx,* D. Pelloquin,† C. Michel,† M. Hervieu,† and B. Raveau†

*EMAT, University of Antwerp (RUCA), Groenenborgerlaan 171, B-2020 Antwerpen, Belgium; and †Laboratoire CRISMAT, ISMRA, Université de Caen, 6 boulevard du Maréchal Juin, 14050 Caen Cedex, France

Received October 13, 1993; in revised form February 17, 1994; accepted February 18, 1994

The structure and defect structure of $Bi_{2-x}Pb_xSr_{3.5}Cu_2(CO_3)O_{8-\delta}$ compounds with $0 \leq x \leq 0.75$ are carefully investigated by electron diffraction and high-resolution electron microscopy. All compounds have an orthorhombic structure with $a \approx b \approx 5.4$ Å and $c \approx 39.5$ Å. The length of the b-axis decreases monotonically with increasing x. The space group for the basic structure is $Abm2$. The structure can be considered as an intergrowth of $Bi_2Sr_2CuO_6$ lamellae with $Sr_2CuO_2(CO_3)$ lamellae along the c-axis. CO_3 groups behave as bridges connecting the CuO_6 octahedra. In the $x = 0$ compound the carbon atoms are shifted away from their symmetry positions; the orientational ordering of the CO_3 groups (or the carbon shift) in successive CO planes alternates along $+b$ and $-b$. Typical Bi-type and Pb-type modulations are found along the b-axis up to a Pb content $x = 0.5$. Electron beam irradiation destroys the ordering of the CO_3 groups and alters the modulated structure.

1. INTRODUCTION

Recently superconductivity was detected in oxycarbonates $Bi_2Sr_4Cu_2(CO_3)O_8$ (1, 2) and $Bi_2Sr_5Cu_3(CO_3)_2O_{10}$ (3). These structures can be considered as intergrowths of the 22 K superconductor $Bi_2Sr_2CuO_6$ (4) and the nonsuperconductor $Sr_2CuO_2(CO_3)$ (5). It is remarkable that the intergrowths have a transition temperature superior to that of the two basic structures; for $Bi_2Sr_4Cu_2(CO_3)O_8$ one finds a T_c of 30 K (1, 2), while for the second compound, $Bi_2Sr_5Cu_3(CO_3)_2O_{10}$, a T_c of 40 K has been measured (3). In spite of this, CO_3 groups have been known to connect the CuO_6 octahedra in the structure, their arrangements and orientations are still not clear.

In all of the compounds studied that are similar to the basic Bi compounds, a one-dimensional modulated structure has been observed. High-resolution electron microscopy (HREM) of the pure Bi compounds has shown that the modulation is mainly located in the double BiO layers (6–8); this idea has been subsequently supported by X-ray and neutron diffraction studies (9, 10). Much discussion has been devoted to the origin of this modulation. A reasonable proposal was made that if the modulation was primarily attributed to the lattice mismatch between the perovskite block and the bismuth oxide lamella, the resulting strain was partially relieved by the accommodation of excess oxygen in the BiO lamella and by the associated creation of holes in the conducting CuO_2 layers. However, it was suggested that the $6s^2$ lone pair of BiIII could also play a role. We will not cite the whole literature here; a survey of the present understanding can be found in (11–13). It is well established that the partial substitution of lead for bismuth drastically changes the modulation; for large a Pb content it tends to disappear (14–17). These experiments suggest that the lone pairs play a prominent role, since it is well known that PbII is much less stereoactive than BiIII. However, a partial oxidation of PbII into PbIV during the synthesis always remains possible. Moreover, the ion radii of PbII and BiIII are different; the substitution may decrease the mismatch as well.

One of the purposes of this paper is to search for a possible CO_3 ordering in the structure. We also studied the evolution of the modulation as a function of the Pb content in the carbonated compounds, $Bi_{2-x}Pb_xSr_{3.5}Cu_2(CO_3)O_{8-\delta}$, for x values between 0 and 0.75. Since the bismuth oxycarbonates have been prepared in sealed tubes, oxygen uptake into the BiO layers is avoided.

No superconductivity was detected in the as-synthesized samples, but after annealing under oxygen pressures of 1 to 40 bars, superconductivity up to 30 K was measured for $x = 0.4$ and $x = 0.5$ (18).

2. SAMPLE PREPARATION

Samples were synthesized from mixtures of the oxides Bi_2O_3, $SrCO_3$, PbO, Sr_2CuO_3, and CuO. The mixtures were prepared in order to have the theoretical composi-

[1] On leave from Beijing Laboratory of Electron Microscopy, Chinese Academy of Sciences, People's Republic of China.

0022-4596/94 $6.00

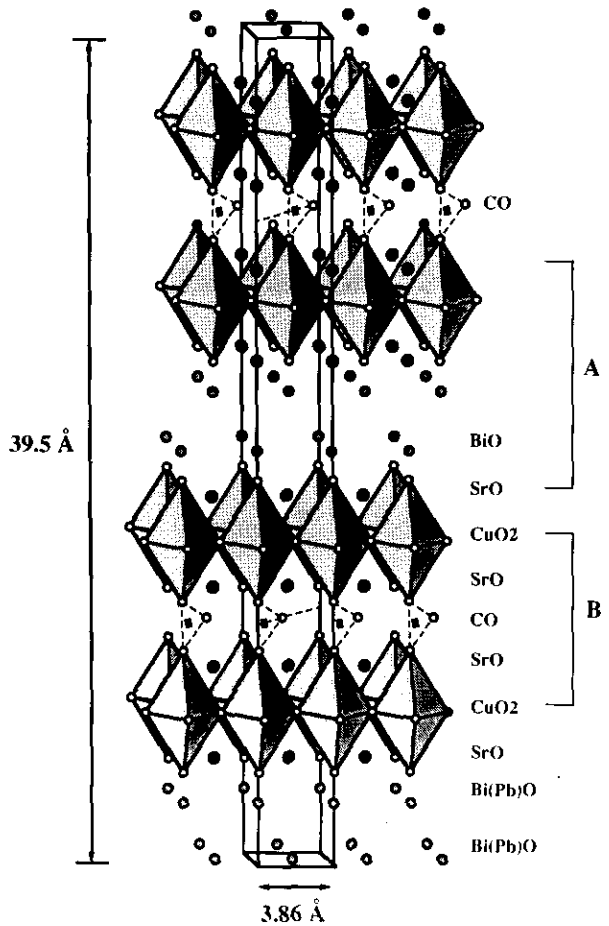

FIG. 1. Schematic representation of the $Bi_{2-x}Pb_xSr_4Cu_2(CO_3)O_8$ structure, without taking into account the orthorhombic deformations and the modulations. Oxygen in BiO planes is ignored in the drawing. The perovskite-based unit cell is outlined. A denotes a 2201 lamella and B denotes a $Sr_2CuO_2(CO_3)$ lamella. Only part of carbon atoms is represented.

tion $Bi_{2-x}Pb_xSr_{3.5}Cu_2(CO_3)O_{8-\delta}$, with $x = 0$, 0.15, 0.25, 0.4, 0.5, 0.75. The compound $Bi_{1.75}Pb_{0.25}Sr_{3.5}Cu_2(CO_3)O_{8-\delta}$ was also prepared starting from PbO_2 rather than from PbO in order to investigate the influence of PbIV on the structural properties of the material. The mixtures were heated for 6 hr at 800°C and quenched to room temperature. Powder X-ray analysis was performed on all samples in order to verify the crystallinity, the purity, and the basic structure. The morphology of the samples was investigated by scanning electron microscopy (SEM).

Samples for transmission electron microscopy (TEM) were crushed and dispersed on a holey carbon grid (Ni and Al for microanalysis and electron diffraction) or directly glued on a copper grid for HREM observations. Observations were made at room temperature, using a Philips 200-kV microscope with ±60° tilt angles or using a Jeol 400-kV high-resolution instrument. Microanalysis measurements were performed on Link equipment. Image simulations of high-resolution observations were performed using the Mac Tempas program.

3. STRUCTURAL ASPECTS OF THE BASIC STRUCTURE

The basic structure of the compound $Bi_2Sr_4Cu_2(CO_3)O_{8-\delta}$ can be described as an intergrowth along the *c*-axis of perovskite blocks with rock salt $SrO–(BiO)_2–SrO$ blocks. The copper single perovskite layers are separated by CO_3 groups; the CO_3 triangular groups behave as bridges and connect the CuO_6 octahedra as illustrated in Fig. 1. The complete structure has been described by Pelloquin *et al.* (1) as a result intergrowth of 2201-type lamellae $Bi_2Sr_2CuO_6$ with $Sr_2CuO_2(CO_3)$-type lamellae. Both building blocks have been indicated as A and B, respectively, in Fig. 1. In this figure, the successive CO_3 groups have been given the same orientation, since no data are as yet available on their exact orientation. The basic pseudo-tetragonal unit cell of 3.8 × 3.8 × 9.5 Å is outlined in Fig. 1, ignoring any lattice modulation, which will be discussed below.

It should be noted that the CO_3 arrangement in one of the component lamellae, the $Sr_2CuO_2(CO_3)$ blocks, has been studied by Miyazaki *et al.* (19) and by Milat *et al.* (20). A superlattice with a unit mesh $2a_p \times 2a_p$, where the index p refers to the perovskite unit cell, has been detected. As we will see, we did not find any indication of this type of superstructure in our compounds. We therefore have to assume that the CO_3 groups behave differently in the intergrowth structure and in the mother phase.

4. RESULTS AND DISCUSSION

4.1. Morphology Studies

Before the TEM investigation, all ceramic samples were investigated by SEM, in order to have an idea of the morphological changes due to Pb substitution. All samples $Bi_{2-x}Pb_xSr_{3.5}Cu_2(CO_3)O_{8-\delta}$ ($x = 0$, 0.25, 0.4, 0.5, and 0.75) consist of plate-like grains (Fig. 2). The grain size is largely independent of the Pb content and on the average about is 10 to 20 μm wide. An exception however is the $x = 0.25$ sample prepared on the basis of PbO_2 (noted $x = 0.25^*$ hereafter). The grain size is considerably smaller than that in the PbO-made samples, and a number of needle-like crystals are distributed among the plate-like grains. Similar needle-like crystals are also found in $x = 0.5$ and $x = 0.75$ samples, but the proportion is much less than that in the $x = 0.25^*$ sample (see Fig. 2). These long needles have been further investigated by TEM; they have

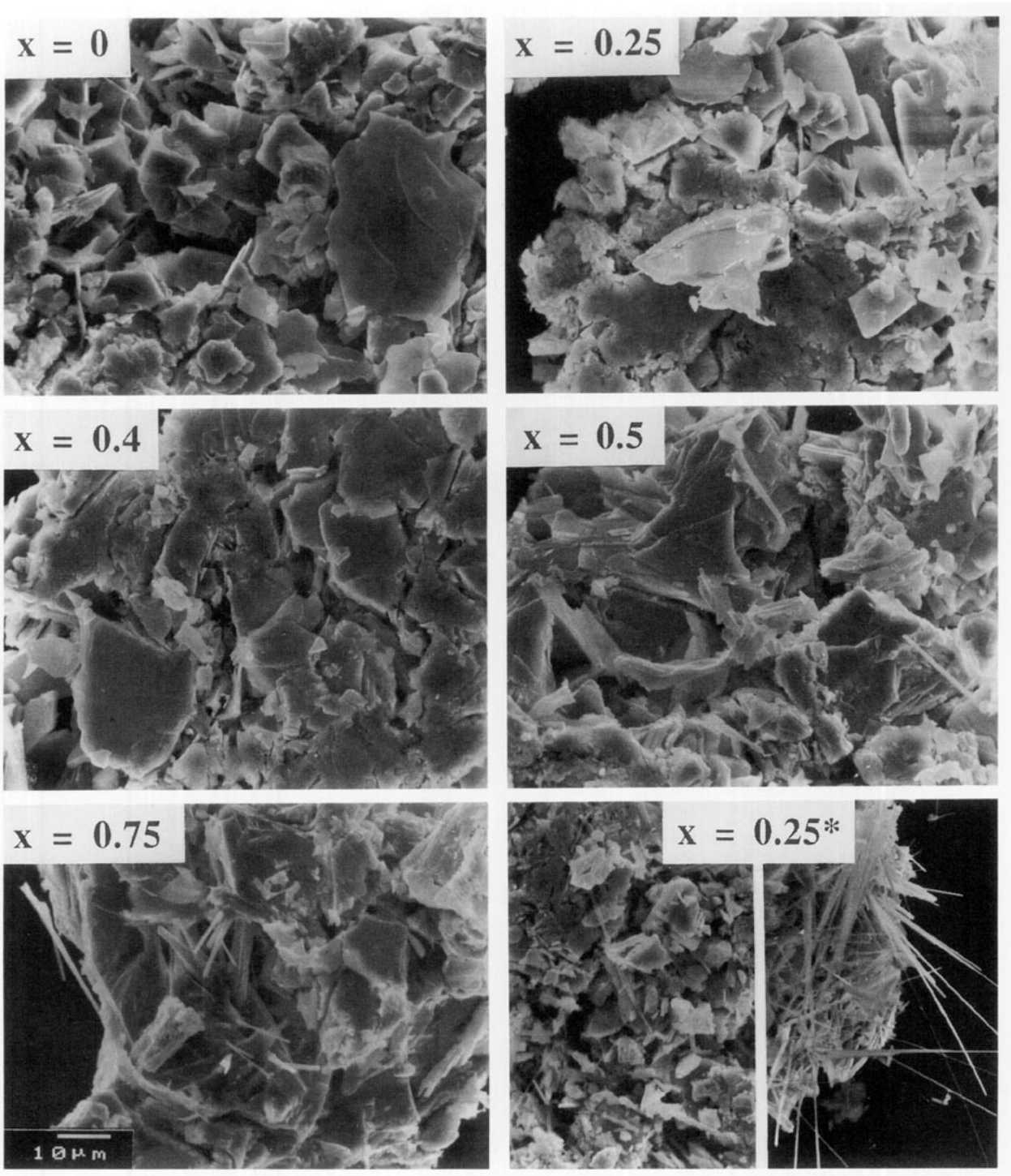

FIG. 2. SEM images of the different $Bi_{2-x}Pb_xSr_{3.5}Cu_2(CO_3)O_{8-\delta}$ samples for the values of x indicated. All images are made at the same magnification; note the needle-like precipitates for $x = 0.25$*.

a hexagonal structure with lattice parameters consistent with the $Sr_5Pb_3CuO_{12}$ structure (21), though Bi is often detected. Presumably PbO_2 is stimulating the growth of Bi-containing $Sr_5Pb_3CuO_{12}$ which relies on PbIV. These $Sr_5Pb_3CuO_{12}$-type crystals thus belong to a foreign phase and will not be considered further.

4.2. Study of the Basic Structure of $Bi_{2-x}Pb_xSr_{3.5}Cu_2(CO_3)O_{8-\delta}$

The X-ray measurements as well as the selected-area electron diffraction (SAED) studies confirm the existence of a solid solution $Bi_{2-x}Pb_xSr_{3.5}Cu_2(CO_3)O_{8-\delta}$ for x values

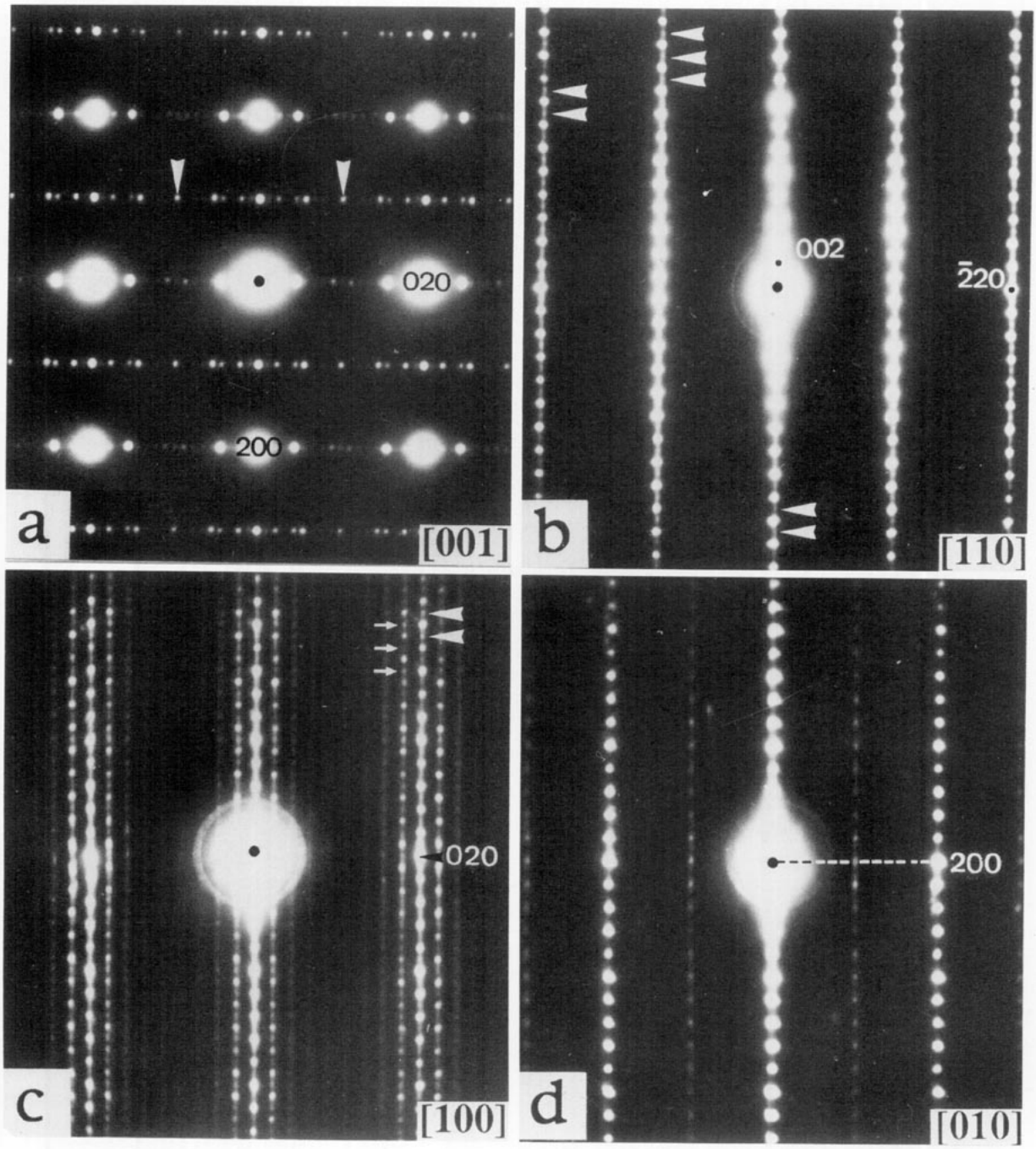

FIG. 3. Series of electron diffraction patterns from the Pb-free sample $Bi_2Sr_{3.5}Cu_2(CO_3)O_{8-\delta}$. Arrowheads indicate some superstructure spots. (a) [001], (b) [110], (c) [100], and (d) [010].

up to 0.75. All patterns can be indexed on an orthorhombic lattice with $a = b \approx 5.45$ Å and $c = 39.5$ Å. The detailed changes of the lattice parameters with the Pb content are shown in Table 1. a does not vary significantly with x, while b decreases monotonically. Similar phenomena have been reported (21, 22, 23). c however reaches a maximum for a composition corresponding to x values between 0.15 and 0.25. This behavior is probably due to the interference of two effects acting in opposite sense; a decrease in size of the cations in the BiO layers reducing c and a decrease of the oxygen content due to the replacement of BiIII by PbII, which increases c.

In the SAED patterns we particularly concentrated on four main zone axes [001], [110], [100], and [010]. In Fig.

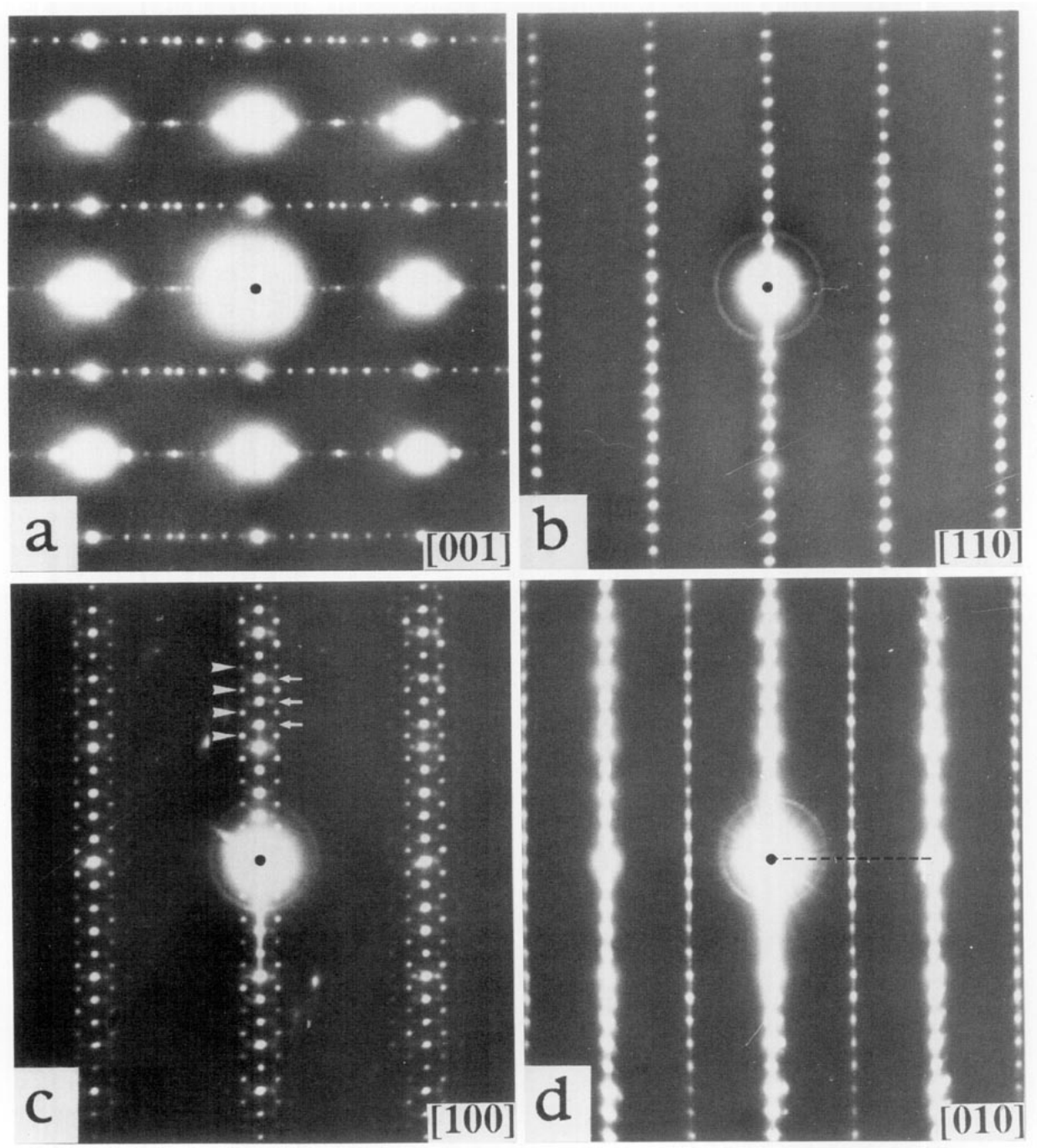

FIG. 4. Same diffraction series as in Fig. 3, but for $Bi_{1.75}Pb_{0.25}Sr_{3.5}Cu_2(CO_3)O_{8-\delta}$. Arrowheads and arrows indicate the Bi-type and Pb-type modulation satellites, respectively. No superstructure spots appear as those indicated in Fig. 3.

3 we show these different sections for the undoped $x = 0$ compound, in Fig. 4 the same sections are shown for the compound $x = 0.25$ (compounds with $x = 0.25$* and $x = 0.4$ show identical patterns), and finally Fig. 5 shows the diffraction pattern as observed in the $x = 0.5$ or $x = 0.75$ compound. The basic reflections in all patterns are clearly consistent with an orthorhombic structure. The Bi-type satellite reflections (see, e.g., (6)) are found in the $x = 0$ sample, while in the $x = 0.25$ and 0.4 samples a mixture of the Bi-type modulation and of the Pb-type modulation is present, as indicated by arrowheads and arrows, respectively, in Fig. 4. In the $x = 0.5$ and 0.75 samples there is hardly any visible modulation, though weak and very diffuse streaks can be identified passing

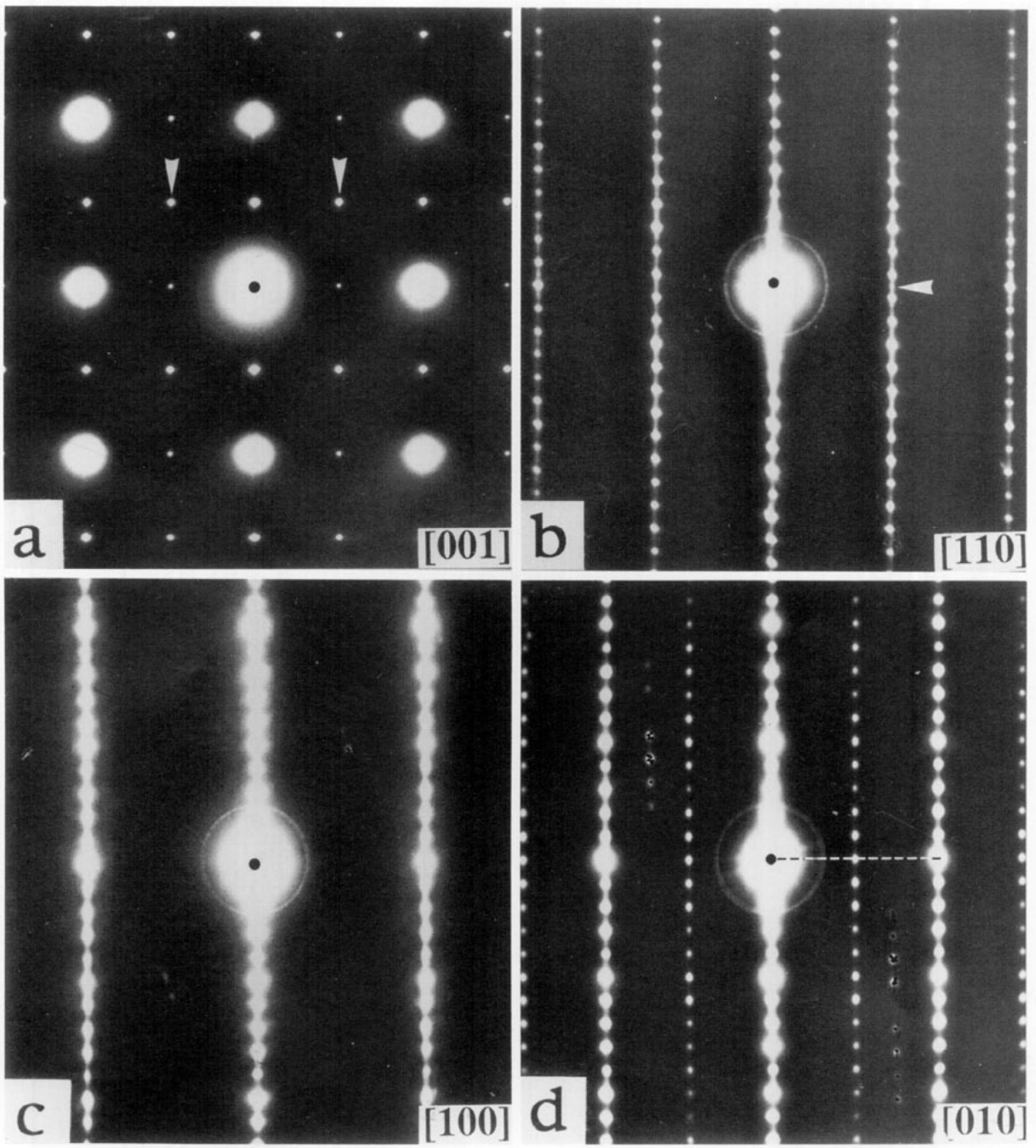

FIG. 5. Same diffraction series as in Fig. 3, but for $Bi_{1.25}Pb_{0.75}Sr_{3.5}Cu_2(CO_3)O_{8-\delta}$. Arrowheads indicate the supplementary reflections.

through each reflection and running along the *b*-axis (see the [100] SAED pattern of Fig. 5). In Fig. 5, some additional spots can be found as indicated which are attributed to a nonhomogeneous Pb distribution in these high-Pb-doped compounds, as we will discuss in the next section.

For each of these compounds, the lattice parameter *a*, *b*, *c*, the modulation wavelength λ, and the modulation vector **q** have been determined directly from the SAED patterns. The variation of the lattice parameters, measured from a submicrometer area, is similar to the average one found macroscopically by X-ray measurements (18). The transition from a pseudo-tetragonal to orthorhombic structure is mainly due to a decrease of *b*. A similar behavior has been reported by Ikeda *et al.* for Bi–Pb–Sr–Cu–O

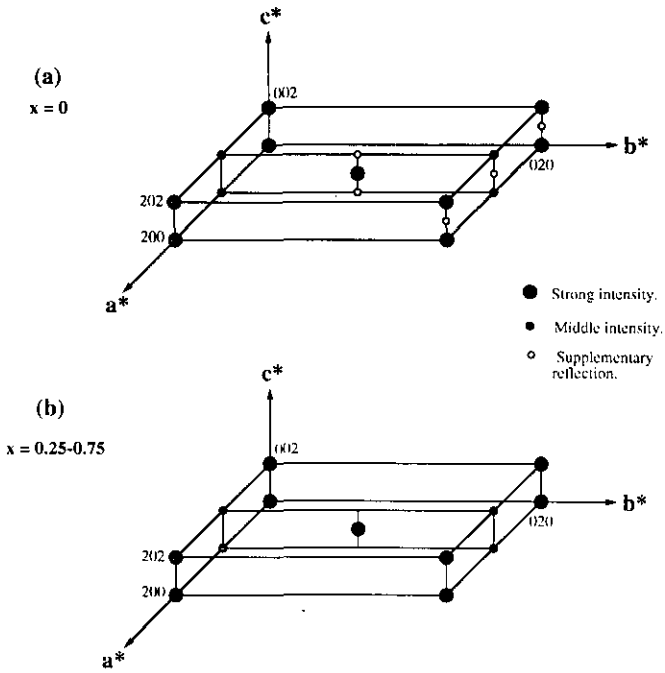

FIG. 6. Reconstruction of the reciprocal lattice for the two different families discussed in Figs. 3, 4, and 5. Large black dots represent perovskite-based reflections, small black dots indicate reflections due to the orthorhombic distortion, and small open circles could be associated with ordering of the CO_3 groups. Reflections due to the modulation have not been indicated in this figure.

compounds (22) and by Flower *et al.* for Bi–Pb–Sr–Ca–Cu–O (23).

By carefully recording different sections of the same sample, the reciprocal space of the basic structure (without modulation) can be reconstructed. As shown in Figs. 3, 4, and 5 we can discern two different cases: (a) for $x = 0$, and (b) for $x = 0.25$ to $x = 0.75$. They are represented schematically in Fig. 6, taking into account the reciprocal unit cell dimensions and the intensity of the reflections. If the additional spots marked by open circles for the $x = 0$ sample, which we will show below are related to an orientational ordering of the CO_3 groups, are not taken into account, the reciprocal spaces for all samples are the same. The reflection conditions for the basic structure are in agreement with the space group *Abm*2 (No. 39).

4.3. The CO_3 Sublattice

The supplementary reflections such as (00*l*), l = odd, marked by small open circles in Fig. 6a, can be observed in the experimental diffraction patterns of Fig. 3. They have been indicated by white arrowheads in the [110] and in the [100] zone-axes SAED patterns (Figs. 3b and 3c). However, they do not appear in the [010] SAED pattern of Fig. 3d. This is clear evidence that these supplementary reflections do not originate from the basic structure. Moreover, the supplementary reflections at (*hhl*), h = odd, l = even, in the [110] pattern of Fig. 3b cannot be explained by double diffraction. Their presence alters the reflection conditions and consequently the symmetry since reflections with (00*l*), l = odd, and (*hhl*), h = even, l = odd, are now allowed. Small arrows in Fig. 3c indicate the additional modulation satellites which do not belong to the Bi-type modulation. They may be caused by double diffraction of the reflections indicated by arrowheads in Fig. 3c.

The CO_3 groups tends to form ordered arrangements as found in similar materials (19, 20). In our case, the intensity of the additional reflections is very weak, and they form a superlattice of the basic lattice; moreover they disappear under electron irradiation. We therefore attribute the extra satellites to a change in the orientation of the CO_3 groups in subsequent layers.

Instead of the fourfold symmetry of the shifts of the carbon atoms in the (001) plane of tetragonal $Sr_2CuO_2(CO_3)$ (18), the carbon sublattice in $Bi_2Sr_{3.5}Cu_2(CO_3)O_{8-\delta}$ could have a lower symmetry because of the orthorhombic environment of the basic structure. If we assume that all carbon atoms within a single (001) plane are to be shifted in the same sense along the preferential

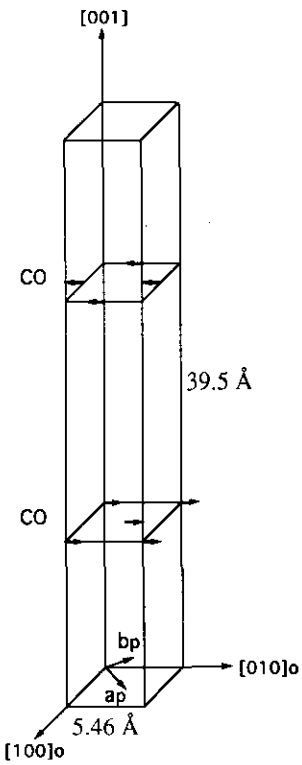

FIG. 7. Schematic representation of the shift of the carbon atoms along successive (001) planes. Only two CO planes are drawn. Small arrows represent the carbon shift directions.

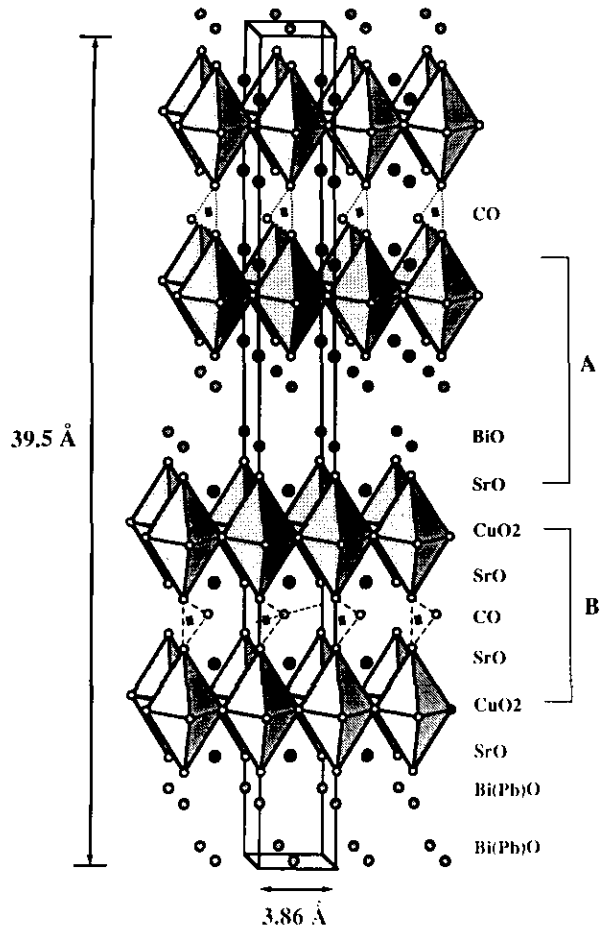

FIG. 8. Structural representation of $Bi_{2-x}Pb_xSr_4Cu_2(CO_3)O_8$ similar to Fig. 1, but with an ordered arrangement of the CO_3 groups in successive CO planes.

$[010]_o$ direction, i.e., the $[110]_p$ direction (subscript "o" refers to $\sqrt{2}a_p \times \sqrt{2}a_p \times c$ orthorhombic structure), but in successive (001) planes along opposite senses (Fig. 7), we change the symmetry. The regular arrangement along the c-axis transforms the A-centered symmetry of the basic structure into a primitive one (Fig. 8). Along the $[110]_o$ or the $[100]_o$ zone axis, this effect will be visible (Fig. 7), and the hhl and $h0l$ reflections (l odd) will appear in the diffraction pattern of Figs. 3b and 3c. Along the $[010]_o$ direction, however, which views the structure parallel to the carbon shifts, the superstructure is not visible, in agreement with the absence of supplementary reflections in the $[010]_o$ zone-axis diffraction pattern of Fig. 3d.

The streaking of the superlattice reflections indicates that considerable disorder is present in the regular alternation of the shift of the carbonate groups. The fact that the reflections disappear under intense irradiation is consistent with the ordering of these carbon shifts; at 400 kV one can easily imagine that as a result of atom displacements the small carbon shifts become uncorrelated and that the superstructure disappears.

High-resolution images of the basic structure can be obtained along the $[1\bar{1}0]$ (or [110]) sections, since in these sections no satellites due to the modulation are present. The result is shown in Fig. 9, and the optical diffraction as well as the calculated image are shown as insets. The simulation is based on the model of Fig. 1, at the Scherzer defocus of −40 nm and for a crystal thickness of 3 nm. A good match has been achieved between this simulation and the experimental image; therefore the black dots in Fig. 9 correspond to the cation columns. One easily recognizes the stacking of the atomic layers according to the sequence ...–BiO–BiO–SrO–CuO_2–SrO–CO–SrO–Cu-O_2–SrO–BiO–..., with a repeat unit of about 39.5 Å along the c direction. Double BiO layers are easily recognized by their very dark contrast, while the carbon layers have the brightest contrast. If we want to image the effect of the carbon shifts, we have to keep in mind that the carbon–oxygen distance in the CO_3 triangle plane is about 1.29 Å (19, 20); the shift of the carbon in the (001) plane is on the order of 0.65 Å, which is far beyond the point resolution of the microscope (1.7 Å for the JEOL 4000 EX). The determination of the configuration of the carbon sublattice by HREM is therefore not straightforward. The less perfect fitting at the position of the CO_3 triangle plane is most probably introduced by local strains and slight cation displacements associated with the pres-

TABLE 1
Lattice Parameters, Wavelength, and Wave Vector Determined by SAED for $Bi_{2-x}Pb_xSr_{3.5}Cu_2(CO_3)O_{8-\delta}$

x	a (Å)	b (Å)	c (Å)	λ_{Bi} (Å) λ_{Pb} (Å)	$\mathbf{q}_{Bi}$ $\mathbf{q}_{Pb}$
0	5.46	5.46	39.3	24.3 (4.45b)	0.22$\mathbf{b}^*$ + $\mathbf{c}^*$
0.25	5.46	5.45	39.6	25.9 (4.78b) 40.0 (7.38b)	0.21$\mathbf{b}^*$ + $\mathbf{c}^*$ 0.14$\mathbf{b}^*$
0.4	5.46	5.44	39.3	24.0 (4.41b) 45.2 (8.31b)	0.23$\mathbf{b}^*$ + $\mathbf{c}^*$ 0.12$\mathbf{b}^*$
0.5	5.46	5.42	39.3	— —	— —
0.75	5.46	5.42	39.6	— —	— —

Note. The camera constant of the electron microscope is calibrated according to the data obtained by powder X-ray diffraction from the same samples (18). $\Delta a = \Delta b \leq \pm 0.04$ Å, $\Delta c = \Delta k \leq \pm 0.4$ Å. λ_{Bi}, wavelength along the b-axis of the Bi-type modulation; λ_{Pb}, wavelength along the b-axis of the Pb-type modulation; $\mathbf{q}_{Bi}$, modulation vector of the B-type modulation; $\mathbf{q}_{Pb}$, modulation vector of the B-type modulation; —, no modulation or only a vague modulation visible.

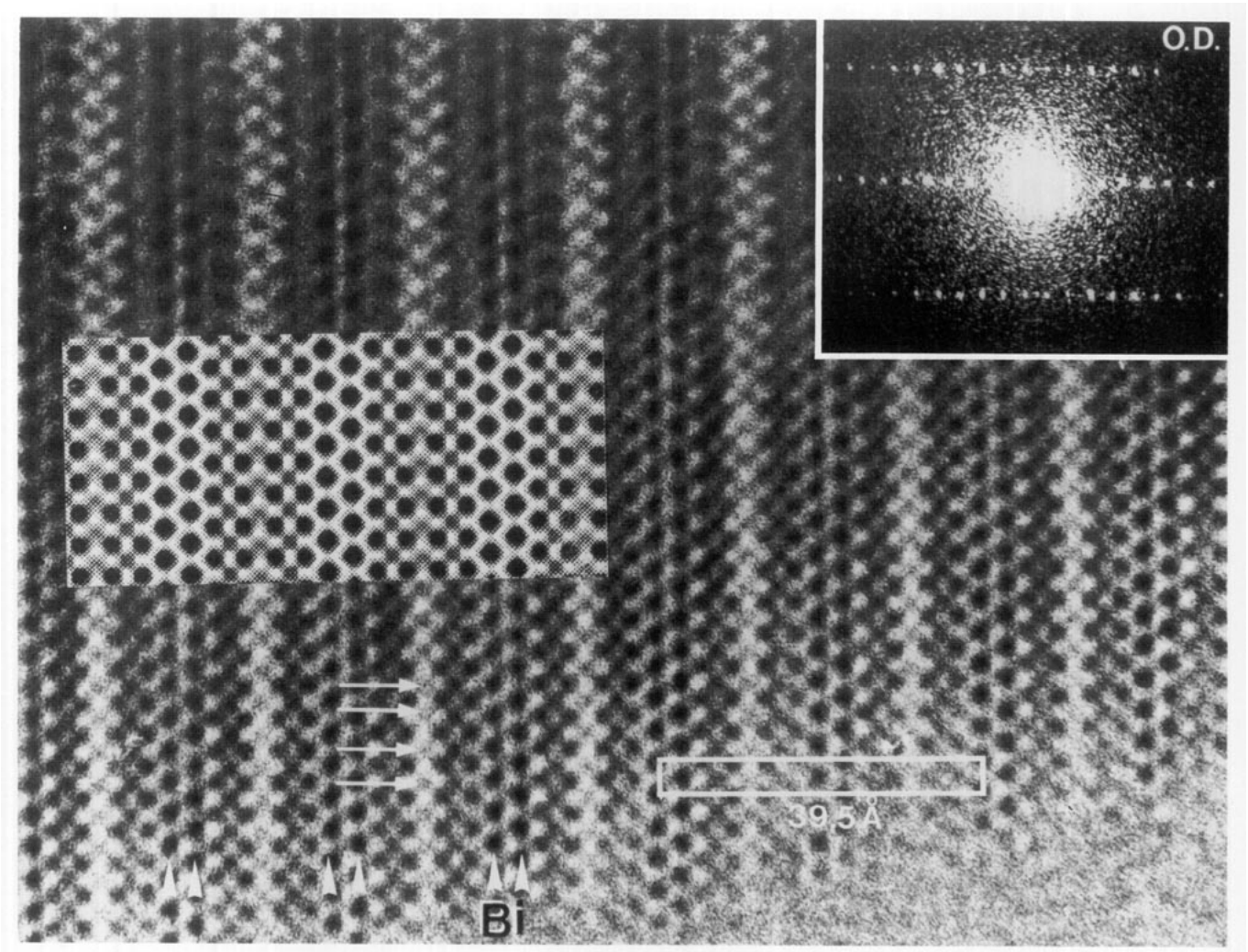

FIG. 9. HREM image along [110], taken close to the Scherzer value of −400 Å. The darker dots correspond to the Bi configuration, while the lighter dots indicate the carbonate groups. The unit cell is outlined. The calculated image for $\Delta f = -400$ Å and a thickness of 30 Å and the optical diffraction pattern are included as an inset.

ence of the CO_3 groups. We have calculated and compared the [110] HREM images for the situation shown in Fig. 1 where all carbon shifts are in the same direction (Fig. 10a) and for the situation shown in Fig. 8 where the carbon atom shifts alternate along the *c*-axis (Fig. 10b). Only very minor changes in the dark dot configuration at the level of the CO plane can be seen. Such minor changes can hardly be expected to be observed in the experimental images. In the Scherzer defocus HREM image of Fig. 9 there are locally some indications of the off-symmetrical location of the dark dots at the CO positions, which could be interpreted as due to the shift of the carbon atoms; they have been indicated by white arrows.

The center of gravity, or the shift direction of the carbon, is probably controlled by the charge distributions due to neighboring ions. Adding Pb to the structure leads to a new charge balance, and the carbon shifts in subsequent carbon layers are affected. They probably become more random, and the additional reflections in the [110] SAED pattern for Pb-free ($x = 0$) sample disappear for Pb-doped samples. Even for the Pb-free sample, electron beam irradiation or *in situ* heating destroys the carbon superstructure. The supplementary reflections are then replaced by streaks, as we discuss in Section 4.6. It should be pointed out that the CO_3 related supplementary reflections appear also in SAED patterns from some regions of $x = 0.5$ and 0.75 samples, as indicated by arrowheads in Fig. 5. This implies a nonhomogeneous Pb distribution in these high-Pb-doped samples.

4.4. Modulated Structure

Satellite reflections can be clearly observed in the [001] and the [100] SAED patterns (a) and (c) of Fig. 3, respectively. For the different compositions, the modulation

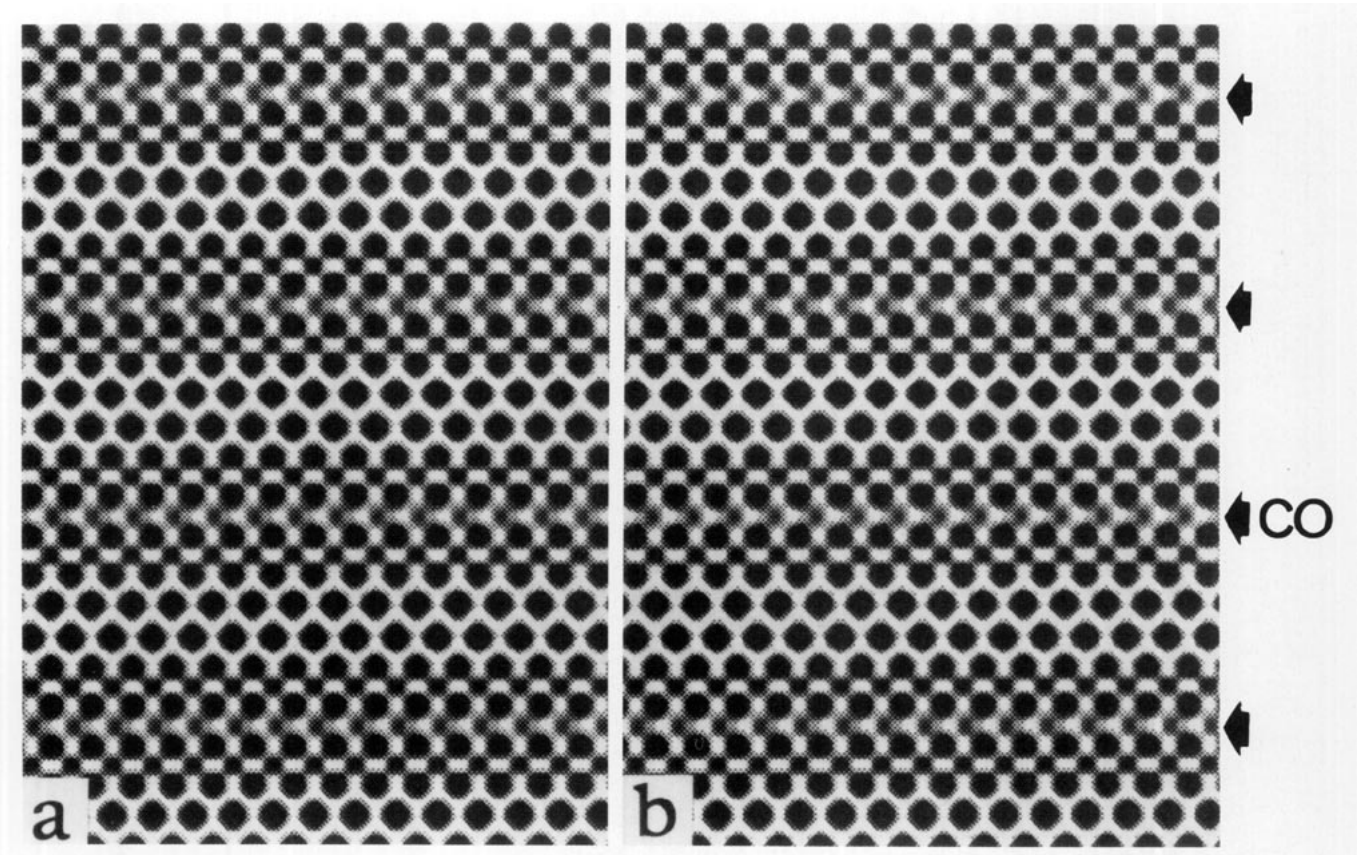

FIG. 10. Calculated [110] images at a thickness of 30 Å and $\Delta f = -400$ Å for two different configurations of the CO_3 groups. (a) All CO_3 groups oriented the same way (Fig. 1); (b) CO_3 groups oriented as presented in Fig. 8.

vectors λ are listed in Table 1. In $x = 0$ sample, only the Bi-type modulation is present, which is characterized by "antiphase" waves predominantly located on the double BiO layers. The cations move along the *b*- and *c*-axes to form the Bi-modulated bands, regions of Bi contraction and regions of Bi expansion. Such observations are well known for $Bi_2Sr_2CaCu_2O_8$ compounds (see, e.g., (6–8)).

For the $x = 0.25$ and 0.4 samples, the diffraction patterns reveal a mixed Bi-type and Pb-type modulation. The Pb-type modulation, which is also mainly located at the level of the (Bi, Pb)O planes, produces "in-phase" waves (15), and the Bi modulation "out-of-phase" waves (e.g., (6–8)). [100] HREM images exhibit the mixed Bi-type and Pb-type modulation; the situation is well represented by Fig. 19c in (6).

In the samples with the highest lead content ($x = 0.5$ and 0.75) the modulation is completely absent in the corresponding diffraction patterns (Fig. 5). However, the Pb-related structures change significantly under electron irradiation, as we will see in Section 4.6.

4.5. Local Modulation and Stacking "Defect" Structures

As mentioned above, the modulation can be regarded as a periodic arrangement of Bi-contracted areas. In the lead-free sample ($x = 0$), the average distance between subsequent contracted regions should be about 4.5 basic units along the *b*-direction. However, as can be seen from the HREM images, a variety of modulation vectors may locally occur. Equivalent regions are therefore no longer aligned along the *c*-axis (as it should be for a modulation vector along b^*) but are shifted along the *b*-axis with respect to each other about one unit length b_O. When these *b*-axis shifts are introduced regularly, additional reflections arise in the [100] SAED pattern, as indicated by white arrowheads in Fig. 3c. More generally, the *A*-centered orthorhombic symmetry is locally destroyed and the local symmetry becomes monoclinic. Such modulation defects have also been observed in the pure Bi samples (24); they produce streaking and contribute to the diffuse character of the satellites in the diffraction pattern.

In general the stacking of the basic Bi oxycarbonate is rather perfect with a periodicity of 39.5 Å; however, stacking errors, particularly in the undoped sample, are regularly encountered. As we have shown, the structure of $Bi_{2-x}Pb_xSr_{3.5}Cu_2(CO_3)O_{8-\delta}$ can be described as the stacking along the *c*-axis of 2201 blocks and $Sr_2CuO_2(CO_3)$ blocks. $Bi_{2-x}Pb_xSr_{3.5}Cu_2(CO_3)O_{8-\delta}$ actually presents the $n = n' = 1$ member of a series $[Bi_{2-x}Pb_xSr_{0-y}Cu_26]_n \cdot [Sr_2$

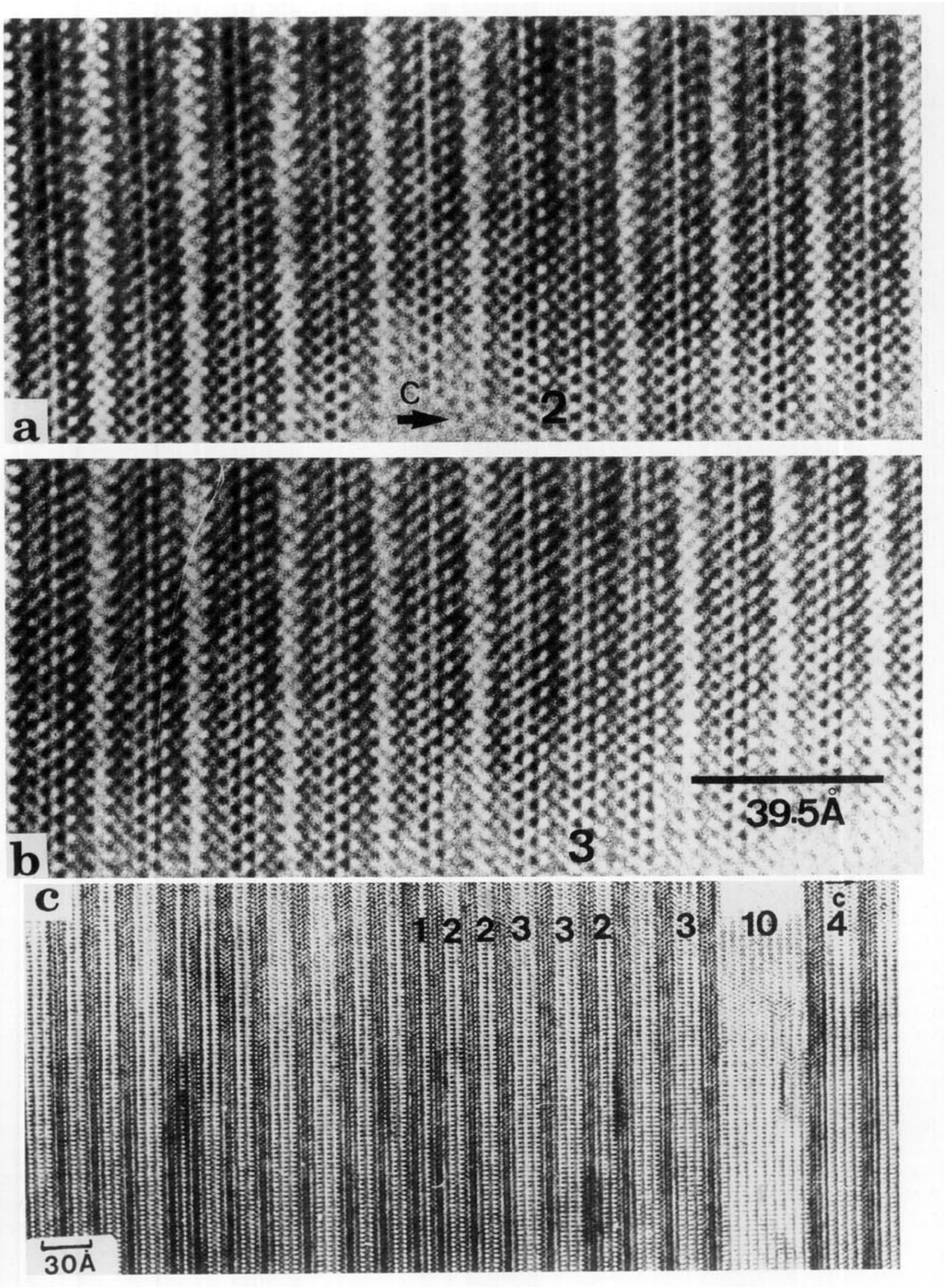

FIG. 11. [110] (a, b) and [010] (c) HREM images of $Bi_2Sr_{3.5}Cu_2(CO_3)O_{8-\delta}$. (a) An extra 2201 block is incorporated into the perfect structure ($n = 2$); (b) two extra 2201 blocks are incorporated ($n = 3$); (c) different numbers of 2201 blocks can be randomly incorporated into the structure.

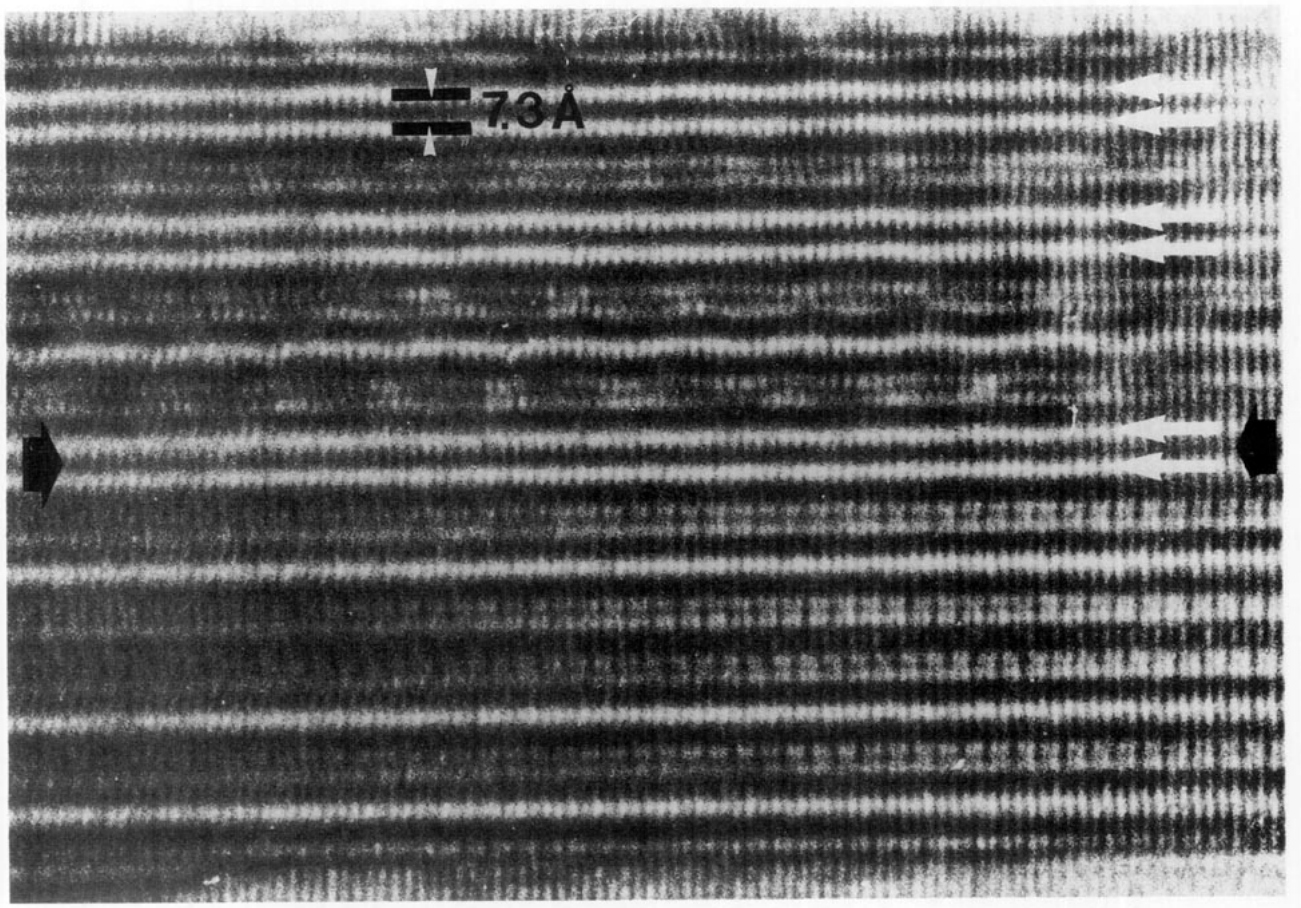

FIG. 12. In the Pb-containing ($x = 0.25$) material local regions of the $n' = 2$ structure, inducing an extra $Sr_2CuO_2(CO_3)$ block between two 2201 blocks, have been regularly observed. Note also the presence of a 90° twin interface at the level of the black arrows. In the top part of the figure the viewing direction is [100], and in the bottom part it is [010]. Growth takes place on a common (001) plane.

$CuO_2(CO_3)]_{n'}$. However, stacking defects occur where two 2201 blocks are inserted between $Sr_2CuO_2(CO_3)$ blocks and where locally the $n = 2$, $n' = 1$ member is formed (Fig. 11a); in other regions (Fig. 11b) three 2201 blocks are in between $Sr_2CuO_2(CO_3)$ slabs, so that the $n = 3$, $n' = 1$ compound is formed. A common feature in the Pb-free sample is apparently the loss of $Sr_2CuO_2(CO_3)$ blocks and the formation of continuous 2201 slabs of variable thickness. In the [010] image of Fig. 11c several n values ranging from 1 to 10 can be observed. In the lead-containing samples this kind of defect has almost never been observed; it seems that adding Pb to the structure reduces this kind of defect lamellae and favors a more homogeneous distribution of the carbonate groups.

In the Pb-containing ($x = 0.25$) material, local regions of the $n = 1$, $n' = 2$ compound have been detected. In this case an extra $Sr_2CuO_2(CO_3)$ block is inserted between two 2201 blocks. CO layers, 7.3 Å apart, rather than the normal 19.5 Å separation, along the c-axis are visible in the image of Fig. 12; the CO layers can be clearly discerned as bright lines. In addition, a 90° rotation twin, located at the position indicated by black arrows, is present in this area. In the top part of the figure the viewing direction is [100]; in the bottom part it is [010]. Growth takes place on a common (001) plane. Such (001) twins have also been observed in the pure Bi compounds (24).

Budin *et al.* (25) recently reported that in Bi–Pb–Sr–Ca–Cu–O, the Bi atoms shift slightly (0.12 Å) away from the rock salt fcc positions along the a direction, resulting in the formation of Bi pairs when viewed along the [010] direction. These Bi pairs form a centered unit mesh in the [010] HREM images, resulting in a *Bbmb* symmetry. However, deviations from this B-centered structure were reported (25). Since the structure and defect structure of $Bi_{2-x}Pb_xSr_{3.5}Cu_2(CO_3)O_{8-\delta}$ are apparently quite analogous to those of $Bi_{2-x}Pb_xSr_2CaCu_2O_y$, in spite of the inserted CO layers, we can expect similar effects in the present compounds. In the [010] HREM image for a compound with $x = 0.5$ this Bi pairing is visible (Fig. 13). In contrast to the B-centered unit mesh observed for Bi_2

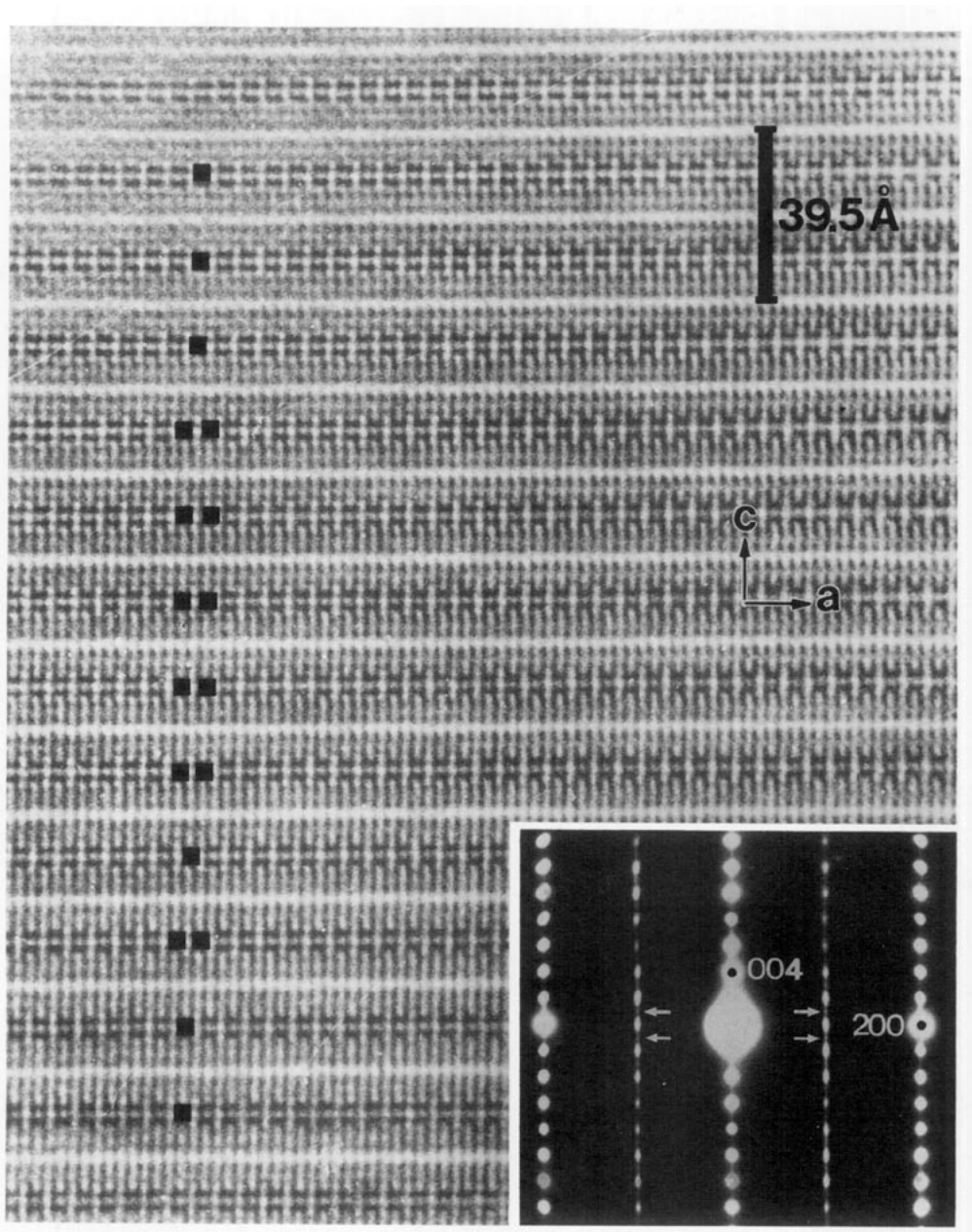

FIG. 13. [010] image of $Bi_{1.5}Pb_{0.5}Sr_{3.5}Cu_2(CO_3)O_{8+\delta}$; the coupling of the Bi positions is clearly visible, giving rise in general to a primitive unit mesh along this projecting direction. Some B-centered unit meshes however are locally observed; they are indicated here. In the electron diffraction pattern the rows h = odd contain the A-type reflections as well as the weak B-type reflections (indicated by small arrows).

$Sr_2CaCu_2O_{8-\delta}$ (25), a primitive unit mesh, i.e., a noncentered unit mesh, is far more abundant in the [010] HREM image of $Bi_{2-x}Pb_xSr_{3.5}Cu_2(CO_3)O_{8-\delta}$; this can be deduced from the [010] diffraction patterns in Figs. 3–5. The projected primitive unit mesh in Fig. 13 actually corresponds to the *A*-centered structure as deduced from the electron diffractions (e.g., Fig. 3). The *A*-centered structure will give rise to reflections at $(h0l)$, $l = 2n$, while a *B*-centered structure would in the same projection produce reflections at $(h0l)$, $h + l = 2n$. In the HREM images however one can locally detect deviations from the *A*-centering; Fig. 13 is consistent with a mixture of *A*-centering and *B*-centering (mixture of primitive and centered meshes composed of Bi pairs). In the diffraction pattern from this area (inset of Fig. 13) both types of $(h0l)$ reflections with l = even and l = odd are visible when h = odd; the reflections corresponding to the *A*-centered symmetry are much stronger, however.

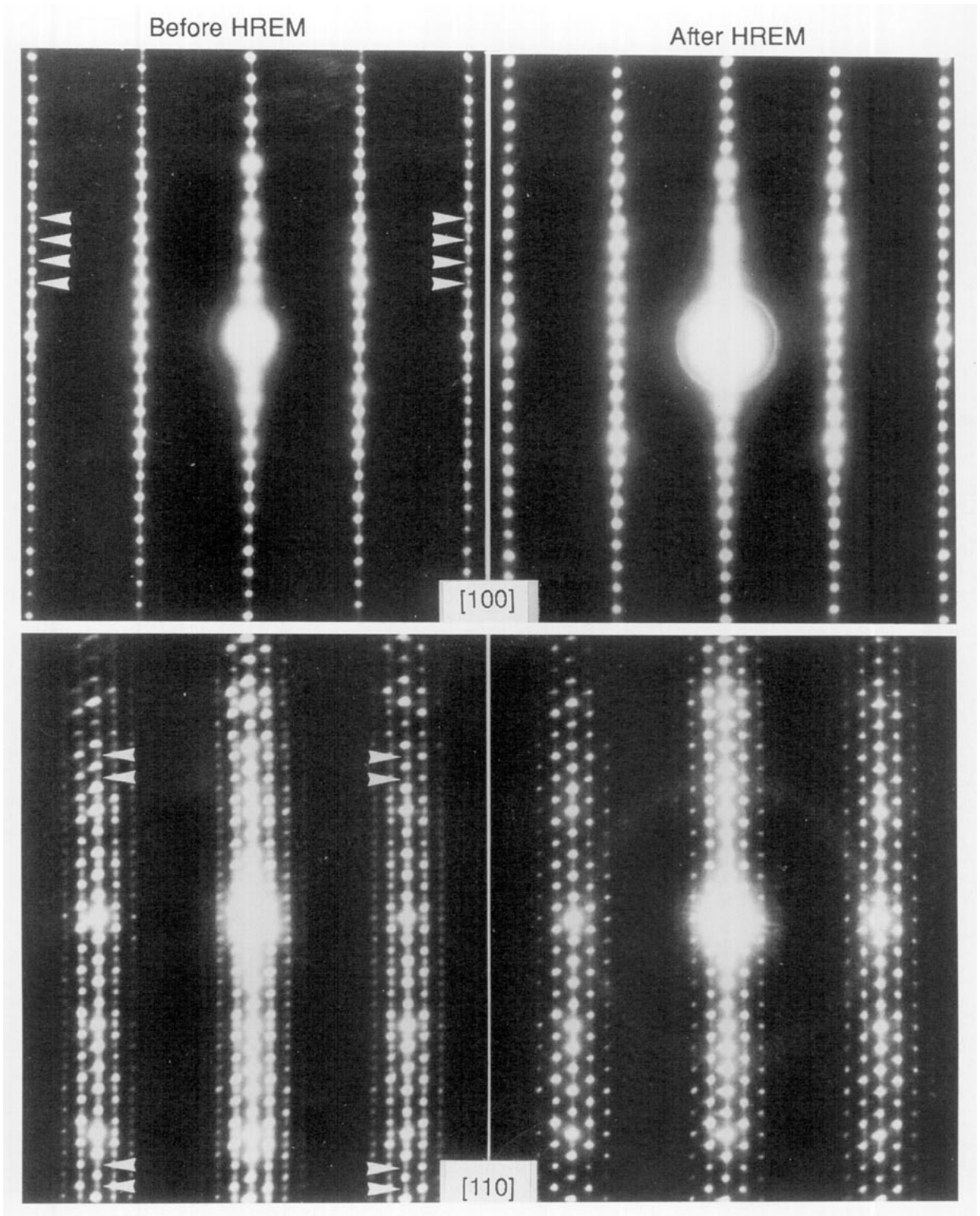

FIG. 14. Disappearance of the supplementary reflections indicated by arrowheads after electron beam irradiation in the [110] and [100] sections.

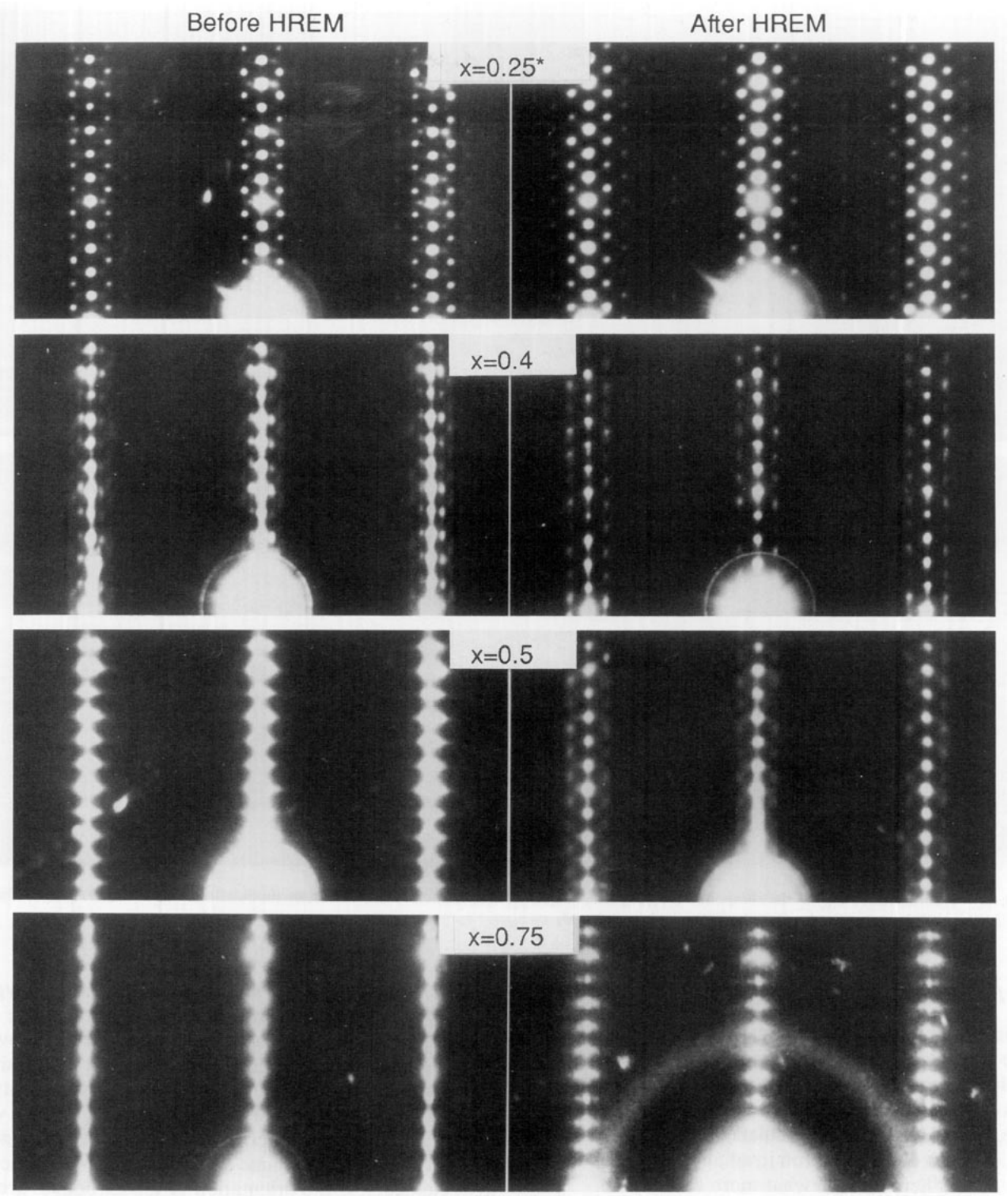

FIG. 15. A change in the modulation of the $Bi_{2-x}Pb_xSr_{3.5}Cu_2(CO_3)O_{8-\delta}$ samples for $x = 0.25$, $x = 0.4$, $x = 0.5$, and $x = 0.75$.

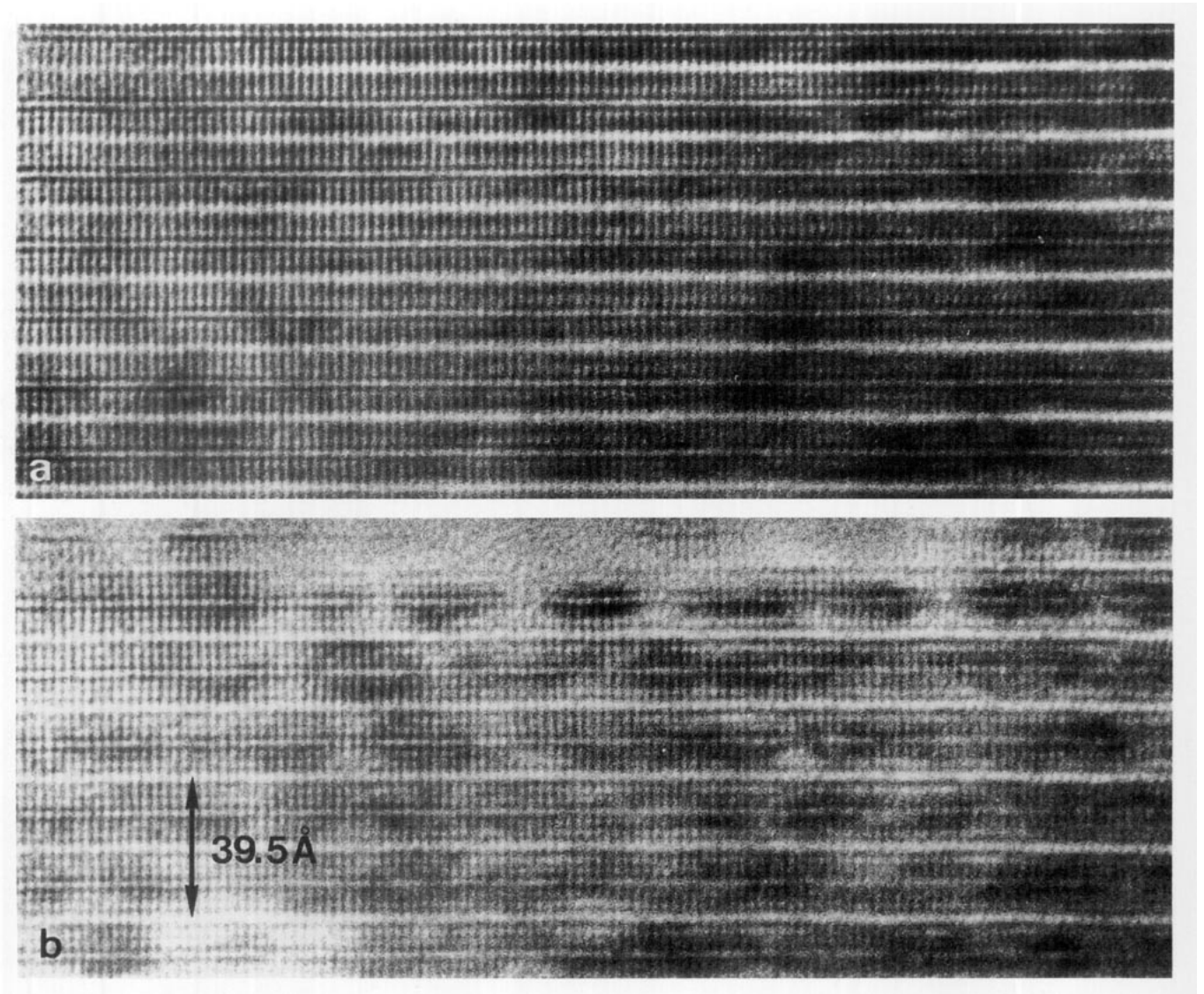

FIG. 16. [100] HREM image of the compound $Bi_{1.25}Pb_{0.75}Sr_{3.5}Cu_2(CO_3)O_{8-\delta}$. (a) before irradiation; no modulation is present. (b) After irradiation at 400 kV; a modulation at the level of the BiO layers is induced.

4.6. Irradiation Effects Due to the Electron Beam

The structure of $Bi_{2-x}Pb_xSr_{3.5}Cu_2(CO_3)O_{8-\delta}$ is found to be sensitive to the 400-kV electron beam. First, the supplementary reflections in the [110], [100] SAED patterns of the $x = 0$ sample vanish upon irradiation. Furthermore, the modulation, particularly the Pb-type modulation, changes during electron irradiation. We will discuss both effects here in somewhat more detail.

Figure 14 shows that the supplementary reflections indicated by arrowheads (see also Fig. 3) before electron beam irradiation are seriously weakened and only a diffuse streak is left after exposing the crystal to an intense electron beam for a few seconds (actually the time to take a HREM image). This is a strong indication that the supplementary reflections are associated with a sublattice of light, mobile elements such as carbon, and/or oxygen. The result is confirmed by the *in situ* heating of the $x = 0$ sample in the microscope. At temperatures as low as 50°C the superstructure reflections disappear irreversibly. At such low temperatures, extensive displacements of heavy atoms such as Bi, Sr, or Cu in the structure are very unlikely, whereas the thermal energy or the momentum transfer is enough to cause a change in the sublattice of light elements. If the orientation of the carbonate groups in successive layers becomes more or less random, streaking of the supplementary spots will result, as has been observed in Fig. 14.

Structure homogenization can be another effect of irradiation. As is known for $Bi_2Sr_2CaCu_2O_y$, the driving force of the modulation is the lattice mismatch between the BiO layers and the perovskite block. Buckling of the BiO

TABLE 2
Irradiation Effects in $Bi_{2-x}Pb_xSr_{3.5}Cu_2(CO_3)O_{8-\delta}$

x	Before irradiation	After 400-kV irradiation
0	Bi-type	Bi-type
0.25	Bi-type and Pb-type	Bi-type
0.4	Bi-type and Pb-type	Bi-type
0.5	Pb-type	Bi-type
0.75	No modulation	Pb-type

layers caused by the atom shifts reduces this lattice mismatch and gives rise to the periodic modulation. Extra space to incorporate extra oxygen in the BiO planes is formed by this mechanism, as proposed by Zandbergen *et al.* (11). The same mechanism should apply and is present, too, for our $Bi_{2-x}Pb_xSr_{3.5}Cu_2(CO_3)O_{8-\delta}$ samples. However, since there is no excess oxygen in our samples due to the vacuum synthesis, these extra spaces remain unoccupied in the structure, leaving a certain mobility to the atoms (in particular in the BiO planes). Local redistribution of the atoms is thus to be expected by electron beam irradiation.

The evolution of the modulated structure has been carefully studied during electron irradiation at 400 kV for each composition $Bi_{2-x}Pb_xSr_{3.5}Cu_2(CO_3)O_{8-\delta}$. Care was taken to focus on exactly the same chosen surface area during the experiment, and the [100] orientation was chosen for all experiments. For the pure Bi-type modulation in the $x = 0$ sample no change is induced, but in the $x = 0.25$, 0.4, 0.5, and 0.75 samples pronounced changes occur. Figure 15 shows an overview of the modulation changes. The mixed Bi-type and Pb-type modulation before irradiation present in the $x = 0.25$ and 0.4 samples is transformed into a Bi-type modulation during irradiation for times less than 1 min (the time needed for focusing and taking a HREM image). For the $x = 0.5$ samples, no apparent modulation exists before irradiation, but a pronounced Bi-type modulation is induced after irradiation; i.e., the Bi-type modulation tends to be reinforced by electron irradiation of $Bi_{2-x}Pb_xSr_{3.5}Cu_2(CO_3)O_{8-\delta}$ samples for $x \leq 0.5$. However, this is no longer the case for strongly Pb-doped samples ($x = 0.75$), where before irradiation no modulation is present but where after irradiation only the Pb-type modulation is observed. There are indications that continued irradiation in this case would transform the Pb-type modulation further to a Bi-type modulation, but the sample is in general degenerating before this occurs. The irradiation results on the different samples are described in Table 2, and the measured modulation vectors before and after HREM are summarized in Table 3.

High-resolution observations of these changes are in general hard to obtain for $x < 0.5$, since the image characteristics change during observation. However, for the $x = 0.5$ or $x = 0.75$ samples, no modulation is present in the initial stage before irradiation (see the SAED of Fig. 5) and the formation of a modulated structure can be followed *in situ*. Figures 16a and 16b show the same area after only 15 sec of irradiation (Fig. 16a) and after 30 sec of irradiation (Fig. 16b). In Fig. 16a there is no visible modulation wave present, while in Fig. 16b a Bi-type modulation is clearly forming; the Bi-contracted regions, producing darker bands in the figure, are clearly visible. Before and after irradiation the chemical composition of the irradiated area was determined by EDX. We found, within the experimental error, no change in the Bi, Pb, Sr, and Cu content of the sample. Carbon and oxygen can be detected in our EDX system, but oxygen changes are too small to be detected, and the low carbon content in the samples cannot be measured quantitatively (not even qualitatively) because of contamination problems. These measurements however confirm that the change in modulation type is not introduced by a change in the chemical composition of the cations in the material, but that the type of modulation is more governed by the local valency of the cations.

5. CONCLUDING REMARKS

We have investigated in great detail the changes in structure of the $Bi_{2-x}Pb_xSr_{3.5}Cu_2(CO_3)O_{8-\delta}$ compounds for different values of x ranging from 0 to 0.75. The symmetry of all samples (not considering the modulation) is orthorhombic. The reflection conditions are in agreement with space group $Abm2$, and the structure can be considered a regular alternation of 2201 lamellae and $Sr_2CuO_2(CO_3)$ lamellae along the c-axis. The CO_3 configuration, connecting the CuO_6 octahedra, introduces a carbon shift along the preferential $[010]_o$ direction. For the $x = 0$ compound, the carbon shifts of successive CO planes alternate along $+[010]_o$ and $-[010]_o$, resulting in the appearance of weak supplementary reflections in the diffraction patterns. This CO_3 orientational ordering is affected consid-

TABLE 3
Modulation Vectors for Different Compositions of $Bi_{2-x}Pb_xSr_{3.5}Cu_2(CO_3)O_{8-\delta}$

x	$\mathbf{q}$Bi	$\mathbf{q}'_{Bi}$	$\mathbf{q}$Pb	$\mathbf{q}'_{Pb}$
0	$0.22\mathbf{b}^* + \mathbf{c}^*$	$0.22\mathbf{b}^* + \mathbf{c}^*$	0	0
0.25	$0.21\mathbf{b}^* + \mathbf{c}^*$	$0.21\mathbf{b}^* + \mathbf{c}^*$	$0.14\mathbf{b}^*$	0
0.4	$0.23\mathbf{b}^* + \mathbf{c}^*$	$0.21\mathbf{b}^* + \mathbf{c}^*$	$0.12\mathbf{b}^*$	0
0.5	0	$0.20\mathbf{b}^* + \mathbf{c}^*$	≈ 0	0
0.75	0	0	0	$9.4\mathbf{b}^*$

Note. $\mathbf{q}$Bi and $\mathbf{q}$Pb are the modulation vectors before irradiation (400 kV), and $\mathbf{q}'_{Bi}$ and $\mathbf{q}'_{Pb}$ are the modulation vectors after several minutes of irradiation.

erably by electron beam irradiation. The time required for taking a single HREM image destroys this carbon modulation. "Normal" Bi-type and Pb-type modulation structures are observed along the *b*-axis and are studied by electron diffraction and HREM. The Pb-type modulation can be seriously weakened by a 400-kV electron beam irradiation, while the Bi-type modulation is generally enhanced, even when no modulation was present before, as in the $x \geq 0.5$ samples. In such complicated structures a number of different defects may occur; they can be connected to the basic structure, the CO_3 group insertion, or the modulated structure.

ACKNOWLEDGMENT

This text presents research results of the Belgian Program on InterUniversity Poles of Attraction initiated by the Belgian State, Prime Ministers Office of Science Policy Programming (IUAP48). The scientific responsibility is assumed by the authors.

REFERENCES

1. D. Pelloquin, M. Caldès, A. Maignan, C. Michel, M. Hervieu, and B. Raveau, *Physica C* **208,** 121 (1993).
2. M. Hervieu, M. Caldès, C. Michel, D. Peloquin, and B. Raveau, *J. Solid State Chem.* **108,** 346 (1994).
3. D. Pelloquin, A. Maignan, M. Caldès, M. Hervieu, C. Michel, and B. Raveau, *Physica C,* **212,** 199 (1993).
4. C. Michel, M. Hervieu, M. M. Borel, A. Grandin, F. Deslandes, J. Provost, and B. Raveau, *Z. Phys. B: Condens. Matter* **68,** 421 (1987).
5. D. V. Formichev, A. L. Kharlanov, E. V. Antipov, and L. M. Kovba, *Superconductivity* **3,** 216 (1990).
6. H. W. Zandbergen, W. A. Groen, A. Smit, and G. Van Tendeloo, *Physica C* **168,** 426 (1990).
7. Y. Matsui and S. Horiuchi, *Jpn. J. Appl. Phys.* **28,** L946 (1989).
8. O. Eibl, *Physica C* **168,** 215 (1990).
9. V. Petricek, Y. Gao, P. Lee, and P. Coppens, *Phys. Rev. B* **42,** 387 (1990).
10. A. Yamamoto, M. Onoda, E. Takayama-Muromachi, and F. Izumi, *Phys. Rev. B: Condens. Matter* **42,** 4228 (1990).
11. H. W. Zandbergen, W. A. Groen, F. C. Mijlhoff, G. Van Tendeloo, and S. Amelinckx, *Physica C* **156,** 325 (1988).
12. G. Calestani, C. Rizzoli, M. G. Francesconi, and G. D. Andreetti, *Physica C* **161,** 598 (1989).
13. H. Zhang and H. Sato, *Physica C* **214,** 265 (1993).
14. J. M. Tarascon, Y. Lepage, W. R. McKinnon, R. Ramesh, M. Eibschutz, E. Tselepis, E. Wang, and G. W. Hull, *Physica C* **172,** 13 (1990).
15. R. Ramesh, K. Ramsching, J. M. Tarascon, and S. M. Green, *J. Mater. Res.* **6,** 278 (1991).
16. C. C. Torardi, E. M. McCarron, P. L. Gai, J. B. Parise, and J. Ghoroghchian, *Physica C* **176,** 347 (1991).
17. G. Calestani, M. G. Francesconi, G. Salsi, G. D. Andreeti, and A. Migliori, *Physica C* **197,** 283 (1992).
18. D. Pelloquin, M. Caldès, C. Michel, A. Maignan, M. Hervieu, and B. Raveau, *Physica C,* **217,** 27 (1993).
19. Y. Miyazaki, H. Yamane, T. Kajitani, T. Oku, K. Hiraga, Y. Hiraga, Y. Morii, K. Fuchizaki, S. Funahashi, and T. Hirai, *Physica C* **191,** 434 (1992).
20. O. Milat, G. Van Tendeloo, S. Amelinckx, T. G. N. Babu, and C. Greaves, *J. Solid State Chem.* **97,** 405 (1992).
21. T. G. N. Babu and C. Greaves, *J. Solid State Chem.* **95,** 417 (1991).
22. Y. Ikeda, Z. Hiroi, H. Ito, S. Shimomura, M. Takano, and Y. Bando, *Physica C* **165,** 189 (1989).
23. N. E. Flower, M. R. Presland, P. Gilberd, and R. G. Buckley, *Physica C* **165,** 161 (1990).
24. G. Van Tendeloo, H. W. Zandbergen, J. Van Landuyt, and S. Amelinckx, *Appl. Phys. A* **46,** 153 (1988).
25. H. Budin, O. Eibl, P. Pongratz, and P. Skalicky, *Physica C* **207,** 208 (1993).